EAI Endorsed Transactions
on Energy Web
Research Article EAI.EU

Data-driven Predictive Individual Pitch Control for Floating Offshore Wind Turbines

Xiaosuo Luo[1,*] and Sergey Gorbachev[2]

[1]School of Artificial Intelligence, Chongqing University of Education, Chongjiao Road, Nanshan Street, Nan'an District, Chongqing, 400065, China
[2] School of Mathematics and Big Data, Chongqing University of Education, Chongjiao Road, Nanshan Street, Nan'an District, Chongqing, 400065, China

Abstract

A method of data-driven predictive individual pitch control is proposed for floating offshore wind turbine. It can reduce platform motion and asymmetric aerodynamic loads effectively. The method is designed, which includes model predictive controller with feedforward compensation, to generate the voltage control signal component required by the pitch mechanism. Firstly, the models of floating offshore wind turbines and wind turbine loads are presented. Then, a model predictive controller utilizes a data-driven methodology grounded in subspace identification for the nonlinear wind turbines. The feedforward compensation with observing past system responses and control experience reduces the external turbulence and enhances the accuracy of the control signal. The simulations indicate that the proposed strategy performs better in terms of reducing fatigue loads and improving the system's stability and reliability.

Keywords: Individual pitch control, Data-driven predictive approach, Floating offshore wind turbine, Nonlinear characteristics

Received on 02 October 2025, accepted on 21 December 2025, published on 22 April 2026

doi: 10.4108/ew.12726

1. Introduction

In recent years, the reserves of fossil fuels are dwindling continuously, environmental pollution is worsening progressively, and the greenhouse effect is intensifying at an accelerating pace. These intertwined environmental and energy challenges collectively pose a critical threat to the sustainable development of society. Consequently, research and development aimed at the rational utilization of renewable energy have become of paramount importance [1]. Wind energy currently holds the second position in the global growth hierarchy of renewable energy installed capacity, with solar energy standing as the top-growing counterpart [2]. Offshore wind power generation has exceeded its onshore equivalent. Furthermore, The presence of vast sea regions with stronger and more stable winds for wind farm development has prompted the engineer to shift toward deep waters to expand farm scales and enhance power extraction. Therefore, for completely utilizing the enormous marine renewable resource, the floating offshore wind turbine (FOWT) represents a transformative approach [3-5].

The preceding references concentrated primarily on environmental loads and motion response. The control of floating wind turbines represents a relatively novel research domain, primarily attributed to the pronounced turbulent winds and unstable platform motions [6-8]. Individual pitch control is an effective method for regulating the output power and load in a wind farm. It is an extremely productive method of ensuring structural and power stability [9]. With the addition of floating platform motions, which increases the turbine's asymmetric load, reducing fatigue loads to ensure a stable wind turbine becomes the priority [10]. Thus, combining individual pitch control with a floating platform to generate deep-water electricity is a promising development

*Corresponding author. Email: lock86@126.com

direction. Accordingly, few works in literature do exist. In this setting, S. Christiansen devised an optimal control strategy for a ballast-stabilized FOWT to achieve a balance between power capture and fatigue [11]. H. Namik and K. Stol primarily designed a periodic state space controller that optimizes power output and platform motions using individual blade pitching [12]. Using the hydraulic pitch actuation system, Venkaiah and Sarkar created a model free fuzzy feedforward PID pitch control method of the horizontal axis wind turbine [13]. Luo proposed a feedback pitch controller for FOWT [14]. However, these methods do not include autonomous learning ability to cope with more complex environments and model-based methods are too dependent on the model accuracy.

The data-driven predictive control methods for wind turbines were appeared in recent years. Navalkar et.al proposed a subspace predictive repetitive control(SPRC) method for load reduction [15]. Liu et.al increased an output constrains with SPRC method for load reduction [16]. In addition, A fault-tolerant SPRC method for individual pitch control was introduced in [17]. But the above wind turbine models were converted into linear time-invariant models without considering the nonlinear characteristics of the wind turbine.

This study proposes an advanced data-driven predictive approach with feedforward compensation. It compares the individual as well as the collective pitch action. The FOWT model with the turbulent wind using a predictive controller versus a traditional controller. It is demonstrated by the results that variable-speed wind turbines integrated with an advanced individual pitch control mechanism exhibit desirable characteristics in power generation and fatigue load mitigation, particularly pertaining to 3P frequency reduction. Subsequently, the fundamental concept examined in this study is critical for providing a reliable and feasible method with increased safety and efficiency for the wind energy industry to further venture into the deep sea. The prominent characteristics of the proposed approach can be outlined as:

- The desired control performance is achieved via a data-driven approach based on subspace identification, eliminating the need for explicit state-space model construction. This method exhibits significantly lower dependency on a priori knowledge and broadens the applicability across diverse scenarios.
- The predictive controller is developed using a nonlinear wind turbine model, replacing the conventional linear time-invariant framework. This design enables superior capability in addressing complex nonlinear problems, outperforming linear models in dynamic system regulation.
- The feedforward compensation is directly integrated into the control input, enabling the system to proactively counteract disturbances before they impact the output. This mechanism enhances real-time disturbance rejection and improves overall control robustness.

The following is the study's organization. Section 2 gives the FOWT model and the fatigue loads, respectively. Section 3 details the progressive controller, while Section 4 contains the simulation. In Section 5, the conclusion is provided.

2. Dynamic model of wind turbine

2.1. Model of FOWT

FOWT dynamics exhibit greater complexity than traditional wind turbines since the degrees of freedom and loads induced. Therefore, the control design of floating platforms and mooring lines has become particularly difficult [18].

This study conducted a comprehensive analysis of FOWT using ADAMS software and constructed a model using FAST, which includes coupled hydraulic and aerodynamic loads in multibody dynamics. The visual FOWT model is given in Figure 1.

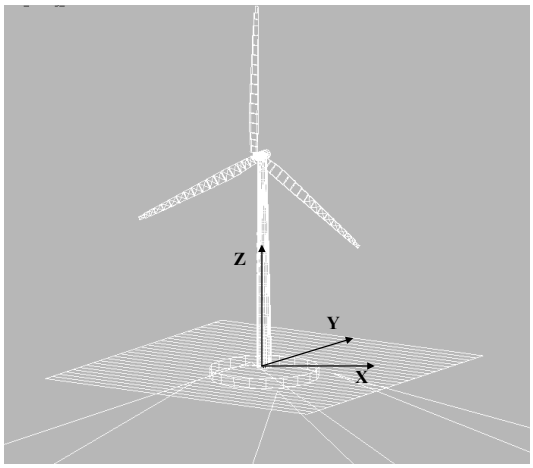

Figure 1. Model of FOWT

This research employed a mooring line stability model within the established framework, implying that all underwater mooring lines are kept under tension. Under the assumption of no seabed contact, horizontal and vertical cable guide coordinates can be derived:

$$x_F(H_F,V_F)=\frac{H_F}{\omega}\left\{\ln\left[\frac{V_F}{H_F}+\sqrt{1+\left(\frac{V_F}{H_F}\right)^2}\right]-\ln\left[\frac{V_F-\omega L}{H_F}+\sqrt{1+\left(\frac{V_F-\omega L}{H_F}\right)^2}\right]\right\}+\frac{H_F L}{EA} \quad (1)$$

$$z_F(H_F,V_F)=\frac{H_F}{\omega}\left\{\sqrt{1+\left(\frac{V_F}{H_F}\right)^2}-\sqrt{1+\left(\frac{V_F-\omega L}{H_F}\right)^2}\right\}+\frac{1}{EA}\left(V_F L-\frac{\omega L^2}{2}\right) \quad (2)$$

The unstretched line length is represented by L, the line weight is denoted by ω, the axial stiffness is given by EA,

the horizontal and vertical components are referred to as H_F, and the vertical component is represented by V_F. In addition, FAST is used to specify the position and detailed tension of each line with other analytical equations.

2.2. Model of wind turbine loads

A suitable wind turbine mathematical model is required to analyze wind turbine loads and design load alleviation controllers. As shown in Figure 2, the drive train experiences acceleration from the aerodynamic driving torque T_a and deceleration from the generator torque T_g:

$$J\dot{\Omega} = T_a - T_g \tag{3}$$

where Ω is the rotor speed and J is the total inertia. Aerodynamic gains are calculated for the linearized effect of pitch angle variation. The pitch angle variation θ_a pitching by the M_{y1} in Figure 2.

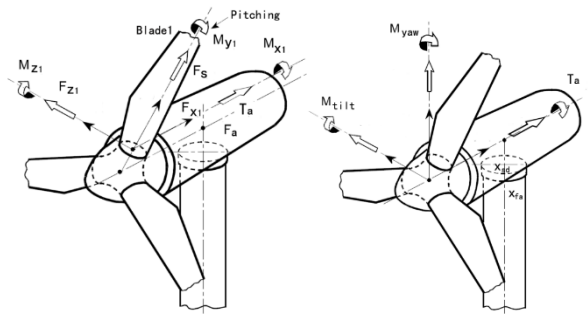

Figure 2. Coordinate system of blade loads and hub loads

$M_{z,i}$ and $M_{x,i}$ denote the fluctuations in flapwise and leadwise blade root bending moments, respectively, while $F_{x,i}$ and $F_{z,i}$ represent flapwise and leadwise forces correspondingly. The gains h_{M_z} … k_{F_z} suggest that the flapwise force per unit span increases with rotor radius while the leadwise force per unit span remains constant.

The fluctuations in aerodynamic torque T_a, rotor tilt moment M_{tilt}, axial force F_a, and tower-top sideward force F_s are subsequently expressed as:

$$\begin{bmatrix} T_a \\ F_a \\ M_{tilt} \\ F_s \end{bmatrix} = \sum_{i=1}^{3} \begin{bmatrix} M_{x,i} \\ F_{x,i} \\ -M_{z,i}\sin\varphi_i \\ -F_{z,i}\sin\varphi_i \end{bmatrix} \tag{4}$$

When the azimuth angle $\varphi = \int_{-\infty}^{t} \Omega_\gamma(\tau)d\tau$ is zero, the first blade is in the horizontal position during its downward rotation. Azimuth angles φ_1, φ_2, and φ_3 of the three blades hold the following:

$$\varphi_1 = \varphi,\ \ \varphi_2 = \varphi + \frac{2\pi}{3},\ \ \varphi_3 = \varphi + \frac{4\pi}{3} \tag{5}$$

Moreover, we can obtain linearized torques and moments:

$$\begin{bmatrix} T_a \\ F_a \\ M_{tilt} \\ F_s \end{bmatrix} = \sum_{i=1}^{3} \begin{bmatrix} h_{M_x} & k_{M_x} & -h_{M_x} \\ h_{F_x} & k_{F_x} & -h_{F_x} \\ -\sin\varphi_i h_{M_z} & -\sin\varphi_i k_{M_z} & -\frac{9R_b}{16H}k_{M_z} \\ -\sin\varphi_i h_{F_z} & -\sin\varphi_i k_{F_z} & -\frac{9R_b}{16H}k_{M_z} \end{bmatrix} \begin{bmatrix} u_i \\ \theta_i \\ \dot{x}_{fa} \end{bmatrix} \tag{6}$$

In this setting, the wind turbine tower and blade dynamics must be included to complete the wind turbine loads model. This adaptability is a result of the large dimensions of its components and the requirement for their low mass. The included tower model has two variables: the sidewards x_{sd} and fore-aft x_{fa}. The tower's fore-aft movement is induced by the aerodynamic tilt moment M_{tilt} and thrust force F_a, whereas the sideward movement.

$$m_{tw}\ddot{x}_{fa} + s_{tw}x_{fa} + d_{tw}\dot{x}_{fa} = F_a - \frac{3}{2H}M_{tilt} \tag{7}$$

$$m_{tw}\ddot{x}_{sd} + s_{tw}x_{sd} + d_{tw}\dot{x}_{sd} = F_s + \frac{3}{2H}T_g \tag{8}$$

In the fore-and-aft and sideward equations of motion, identical values for the tower top equivalent mass m_{tw}, spring constant s_{tw}, and damper constant d_{tw} apply. These measurements are based on structural data such as the horizontal tower displacement at unity force, first bending mode damping rate, and first fore-and-aft and sideward frequency averages.

Finally, a conclusion is drawn from the preceding expressions:

$$J\dot{\Omega} = h_{M_z}\sum_{i=1}^{3}u_i + k_{M_x}\sum_{i=1}^{3}\theta_i - 3h_{M_x}\dot{x}_{fa} - T_g \tag{9}$$

$$M_{zi} = h_{M_z}\left(\sin\varphi_i\frac{9R_b}{8H} - 1\right)\dot{x}_{fa} + h_{M_z}u_i + k_{M_z}\theta_i \tag{10}$$

3. Design of Control Strategy

3.1. State space equations and overall control framework

In an offshore system, the controller's design should prioritize turbulence. When winds and waves have an effect, the waves' effect is frequently referred to as tower acceleration, and it is

explicitly represented in the control design. Finally, waves are created by the wind, which dominates the floating platform's response. So we assume that the load on the floating platform is all considered as a nonlinear load with irregular line breaks. We design a random model to represent the load signal obtained based on blade changes. Using the model of the influence of wind speed changes as a variation of tower modes, the load signal $v(k)$ is defined as follows:

$$v(k+1) = v(k) + w(k) \tag{11}$$

where $w(k)$ is a generalized disturbance signal that contains the wave periodic impact as a random Gaussian white noise with a mean of zero and a covariance matrix. With transformed M_{tilt} and M_{yaw}, the individual control aims to reduce the asymmetrical air torque with turbulence wind above the rated wind speed. It entails that the objective functions M_{tilt} and M_{yaw} are attempted to track to zero. Due to the internal coupling and the presence of multiple variables, traditional SISO controllers are incapable of meeting the system's requirements. Hence, combining the wind turbine models discussed in Section 2:

$$\begin{cases} \begin{bmatrix} x(k+1) \\ v(k+1) \end{bmatrix} = \begin{bmatrix} A & B_v \\ 0 & I \end{bmatrix} \begin{bmatrix} x(k) \\ v(k) \end{bmatrix} + \begin{bmatrix} B_u \\ 0 \end{bmatrix} u(k) + \begin{bmatrix} w_x(k) \\ w_v(k) \end{bmatrix} \\ y(k) = \begin{bmatrix} C & 0 \end{bmatrix} \begin{bmatrix} x(k) \\ v(k) \end{bmatrix} + \begin{bmatrix} D \\ 0 \end{bmatrix} u(k) + w_y(k) \end{cases} \tag{12}$$

where $y = \begin{bmatrix} M_{tilt} & M_{yaw} \end{bmatrix}$ represents the observation output, $u = \begin{bmatrix} \theta_1 & \theta_2 & \theta_3 \end{bmatrix}$ represents the control input. The system state variable x contains the states of the wind turbine model, torque control, and pitch control. A, B_v, B_u, C, D are the system state space matrices and I is the identity matrix. The system's state is estimated using the Kalman filter, and the estimate signal has a significant effect on the controller. It can be demonstrated that the above-mentioned state space is significantly large. The feedforward-based data-driven control strategy is considered in the presence of turbulence wind. The system's feedforward is responsible for storing and correcting the strategy's state and control variables. In this setting, the Kalman filter receives system measurement signals such as the FOWT's computed yaw and tilt moments and the current time, and estimates the three blades' individual wind speeds and state variables x. Thus, using the data-driven controller, the untreated pitch angle is obtained. Alternatively, the pitch angle command provides feedback to the Kalman Filter during its estimation process. As proposed, the feedforward stores data up to the present moment and history data for the discrete system.

Thus, the ultimate pitch angle is then calculated using two components: standard data-driven predictive control u^c and feedforward-based compensation $F(z)$.

$$u = u^c + F(z) \tag{13}$$

3.2. Data-driven predictive control with feedforward compensation

Eq. (12) can be written in the following nonlinear form:

$$\begin{cases} x(k+1) = Ax(k) + B_v v(k) + B_u u(k) + w_x(k) \\ y(k) = Cx(k) + Du(k) + w_y(k) \end{cases} \tag{14}$$

where k is the current time. Define f is the length of the future time, and Eq. (14) can be transformed through iteration:

$$y_f = \Gamma_f x(k) + K_f v_f + H_f u_f + G_f w_{xf} + w_{yf} \tag{15}$$

where the extended observability matrix Γ_f, Toeplitz matrices K_f, H_f, G_f and system vectors y_f, u_f, v_f, w_{xf}, w_{yf} are:

$$\Gamma_f = \begin{bmatrix} C \\ CA \\ \mathrm{M} \\ CA^{f-1} \end{bmatrix}, K_f = \begin{bmatrix} D & 0 & \mathrm{L} & 0 \\ CB_v & D & \mathrm{O} & \mathrm{M} \\ \mathrm{M} & \mathrm{O} & \mathrm{O} & 0 \\ CA^{f-2}B_v & \mathrm{L} & CB_v & D \end{bmatrix},$$

$$H_f = \begin{bmatrix} D & 0 & \mathrm{L} & 0 \\ CB_u & D & \mathrm{O} & \mathrm{M} \\ \mathrm{M} & \mathrm{O} & \mathrm{O} & 0 \\ CA^{f-2}B_u & \mathrm{L} & CB_u & D \end{bmatrix},$$

$$G_f = \begin{bmatrix} 0 & 0 & \mathrm{L} & 0 \\ C & 0 & \mathrm{L} & 0 \\ \mathrm{M} & \mathrm{O} & \mathrm{O} & \mathrm{M} \\ CA^{f-2} & \mathrm{L} & CA & 0 \end{bmatrix}, \quad y_f = \begin{bmatrix} y(k) \\ y(k+1) \\ \mathrm{M} \\ y(k+f-1) \end{bmatrix},$$

$$u_f = \begin{bmatrix} u(k) \\ u(k+1) \\ \mathrm{M} \\ u(k+f-1) \end{bmatrix}, \quad w_{xf} = \begin{bmatrix} w_x(k) \\ w_x(k+1) \\ \mathrm{M} \\ w_x(k+f-1) \end{bmatrix},$$

$$w_{yf} = \begin{bmatrix} w_y(k) \\ w_y(k+1) \\ \mathrm{M} \\ w_y(k+f-1) \end{bmatrix}.$$

The Eq. (15) can be denoted using Hankel matrices:

$$Y_f = \Gamma_f X_f + K_f V_f + H_f U_f + G_f W_{xf} + W_{yf} \tag{16}$$

At the past time p, the Hankel matrices can be expressed as

$$Y_p = \Gamma_p X_p + K_p V_p + H_p U_p + G_p W_{xp} + W_{yp} \tag{17}$$

The output Hankel matrices are presented as

$$Y_f = \begin{bmatrix} y(k) & y(k+1) & \mathrm{L} & y(N-f+1) \\ y(k+1) & y(k+2) & \mathrm{L} & y(N-f+2) \\ \mathrm{M} & \mathrm{M} & \mathrm{O} & \mathrm{M} \\ y(k+f-1) & y(k+f) & \mathrm{L} & y(N) \end{bmatrix},$$

$$Y_p = \begin{bmatrix} y(k-p) & y(k-p+1) & \cdots & y(N-f-p+1) \\ y(k-p+1) & y(k-p+2) & \cdots & y(N-f-p+2) \\ \vdots & \vdots & \ddots & \vdots \\ y(k-1) & y(k) & \cdots & y(N-f) \end{bmatrix}.$$

where N is the sampling time. Similarly, U_f, U_p, V_f, V_p, W_{xf}, W_{xp}, W_{yf}, and W_{yp} have similar definitions. Extended observability matrix Γ_p and Toeplitz matrices K_p, H_p, G_p are:

$$\Gamma_p = \begin{bmatrix} C \\ CA \\ \vdots \\ CA^{p-1} \end{bmatrix}, \quad K_p = \begin{bmatrix} D & 0 & \cdots & 0 \\ CB_v & D & \ddots & \vdots \\ \vdots & \ddots & \ddots & 0 \\ CA^{p-2}B_v & \cdots & CB_v & D \end{bmatrix},$$

$$H_p = \begin{bmatrix} D & 0 & \cdots & 0 \\ CB_u & D & \ddots & \vdots \\ \vdots & \ddots & \ddots & 0 \\ CA^{p-2}B_u & \cdots & CB_u & D \end{bmatrix},$$

$$G_p = \begin{bmatrix} 0 & 0 & \cdots & 0 \\ C & 0 & \cdots & 0 \\ \vdots & \ddots & \ddots & \vdots \\ CA^{p-2} & \cdots & CA & 0 \end{bmatrix}.$$

The state vectors are

$$X_f = \begin{bmatrix} x(k) & x(k+1) & \cdots & x(N-f+1) \end{bmatrix},$$

$$X_p = \begin{bmatrix} x(k-p) & x(k-p+1) & \cdots & x(N-f-p+1) \end{bmatrix}.$$

The optimal prediction output can be represented by the subspace matrices as

$$Y_f = L_w W_p + L_v V_f + L_u U_f \tag{18}$$

where W_p is denoted as the past input-output data matrix: $W_p = [Y_p^{\mathrm{T}} \quad V_p^{\mathrm{T}} \quad U_p^{\mathrm{T}}]^{\mathrm{T}}$, L_w, L_v, L_u are subspace matrices obtained from block Hankel matrices:

$$\min_{L_w, L_u} \left\| Y_f - (L_w, L_v, L_u) \begin{pmatrix} W_p \\ V_f \\ U_f \end{pmatrix} \right\|_F^2 \tag{19}$$

where $\|\cdots\|_F$ is the Frobenius norm. It can be obtained as:

$$\hat{Y}_f = Y_f / \begin{pmatrix} W_p \\ V_f \\ U_f \end{pmatrix} \tag{20}$$

where / is the orthogonal projection. Performe a QR-decomposition:

$$\begin{bmatrix} W_p \\ V_f \\ U_f \\ Y_f \end{bmatrix} = R^{\mathrm{T}} Q^{\mathrm{T}} = \begin{bmatrix} R_{11} & 0 & 0 & 0 \\ R_{21} & R_{22} & 0 & 0 \\ R_{31} & R_{32} & R_{33} & 0 \\ R_{41} & R_{42} & R_{43} & R_{44} \end{bmatrix} \begin{bmatrix} Q_1^{\mathrm{T}} \\ Q_2^{\mathrm{T}} \\ Q_3^{\mathrm{T}} \\ Q_4^{\mathrm{T}} \end{bmatrix} \tag{21}$$

where Q and R are orthogonal matrix and low triangular matrix. Set:

$$L = \begin{bmatrix} R_{41} & R_{42} & R_{43} \end{bmatrix} \begin{bmatrix} R_{11} & 0 & 0 \\ R_{21} & R_{22} & 0 \\ R_{31} & R_{32} & R_{33} \end{bmatrix}^{\dagger} \tag{22}$$

with

$$L = \begin{bmatrix} L_w & L_v & L_u \end{bmatrix} \tag{23}$$

where $L_w \in \mathrm{R}^{fl \times p(m+l)}$, $L_v \in \mathrm{R}^{fl \times fm}$, $L_u \in \mathrm{R}^{fl \times fm}$ and superscript $\dagger$ is the Moore-Penrose pseudo-inverse.

Solving the model predictive control (MPC) problem involves minimizing a cost function. A representative cost function form in MPC is presented as follows:

$$J = \sum_{k=1}^{N_p} (\hat{y}_{t+k} - r_{t+k})^{\mathrm{T}} Q (\hat{y}_{t+k|t} - r_{t+k}) + \sum_{k=1}^{N_c} \Delta v_{t+k-1}^{\mathrm{T}} R_v \Delta v_{t+k-1} + \sum_{k=1}^{N_c} \Delta u_{t+k-1}^{\mathrm{T}} R_u \Delta u_{t+k-1} \tag{24}$$

where Q, R_v, and R_u are the weight matrices. Increasing the Q can make the actual output approach the target trajectory faster, but the overshoot may increase. Increasing R_v and R_u can reduce the amplitude of the control input and decrease energy consumption, but may sacrifice system response speed. A balance needs to be struck between "speed" and "economy". The reference setpoint signal at the current time is r_t, with N_p and N_c denoting the prediction horizon and control horizon respectively. Eq. (24) can be rewrite as

$$J = \left(\hat{y}_f - r_f\right)^{\mathrm{T}} Q \left(\hat{y}_f - r_f\right) + \Delta v_f^{\mathrm{T}} R_v \Delta v_f + \Delta u_f^{\mathrm{T}} R_u \Delta u_f \tag{25}$$

The predict output in MPC framework is:

$$\hat{y}_f = F_l y_t + \Gamma_l L_w \Delta w_p + \Gamma_l L_v \Delta v_f + \Gamma_l L_u \Delta u_f \tag{26}$$

where $F_l = \begin{bmatrix} I_l^{\mathrm{T}} & \cdots & I_l^{\mathrm{T}} \end{bmatrix}^{\mathrm{T}}$, $\Gamma_l = \begin{bmatrix} I_l & 0 & \cdots & 0 \\ I_l & I_l & \cdots & 0 \\ \vdots & \vdots & \ddots & \vdots \\ I_l & I_l & \cdots & I_l \end{bmatrix}$,

$$\Delta u_f = \begin{bmatrix} \Delta u_t^{\mathrm{T}} & \Delta u_{t+1}^{\mathrm{T}} & \cdots & \Delta u_{t+f-1}^{\mathrm{T}} \end{bmatrix}^{\mathrm{T}},$$

$$\Delta v_f = \begin{bmatrix} \Delta v_t^{\mathrm{T}} & \Delta v_{t+1}^{\mathrm{T}} & \cdots & \Delta v_{t+f-1}^{\mathrm{T}} \end{bmatrix}^{\mathrm{T}},$$

$$\Delta w_p = \begin{bmatrix} \Delta y_{t-p+1}^{\mathrm{T}} & \cdots & \Delta y_t^{\mathrm{T}} & \Delta u_{t-p}^{\mathrm{T}} & \cdots & \Delta u_{t-1}^{\mathrm{T}} \end{bmatrix}^{\mathrm{T}}.$$

Substituting the predictor in Eq. (26) into the cost function in Eq. (25), differentiate it with respect to Δu_f and control sequence can be obtained:

$$\Delta u_f = -\left((\Gamma_l L_u)^{\mathrm{T}} Q (\Gamma_l L_u) + R\right)^{-1} \times \left(\Gamma_l L_u\right)^{\mathrm{T}} Q \left(\Gamma_l L_w \Delta w_p + \Gamma_l L_v \Delta v_f + F_l (y_t - r_t)\right) \tag{27}$$

At each time step, the control input u_k^c is depicted as

$$u_k^c = u_{k-1}^c + \Delta u_k \tag{28}$$

To improve the control's accuracy and reliability, usually, the feedforward control manually adjusts the ultimate pitch angle. By constantly storing and learning, the feedforward compares the incoming signal to the recorded one. When the ultimate pitch angle signal is sent to the actuator, it is adjusted. According to Eq. (14), the following transformation equation can be obtained:

$$G(z) = C(zI - A)^{-1} B_u + D \tag{29}$$

$$H(z) = C(zI - A)^{-1} B_v \tag{30}$$

where $G(z)$ and $H(z)$ are transformation matrices. Thus, the system feedback laws were obtained with the zero-mean random process $v(k)$:

$$y(k) = G(z)u(k) + H(z)v(k) + w_y(k) \tag{31}$$

Design the following feedforward control law:

$$u(k) = F(z)v(k) \tag{32}$$

The feedforward controller $F(z)$ should be designed to minimize the influence of $v(k)$ on $y(k)$, implying that to make the motion track zero, the feedforward controller should obey $y = 0$. Therefore, the feedforward controller is given as:

$$F(z) = -H(z)G^{-1}(z) \tag{33}$$

Figure 3 illustrates the control system block diagram.

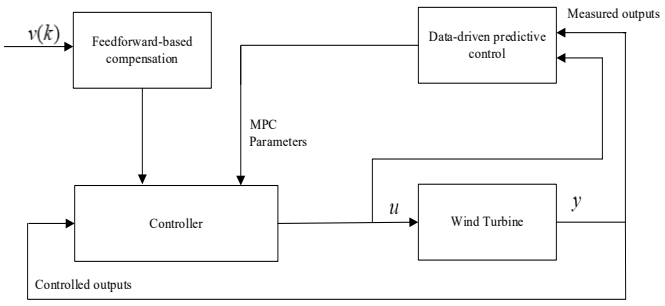

Figure 3. The control system block diagram

4. Simulation

The simulation environment was developed using FAST and MATLAB. The model established in FAST was employed. A 5 MW offshore floating wind turbine was modeled in FAST under an average turbulent wind speed of 11 m/s. Various parameters of the floating platform are shown in Table 1. It should be noted that these data and parameters are random and have not undergone generalization training.

Table 1. Parameters of floating platform

Variable	Numerical value
Rotor radius	63m
Rotor quality	110000Kg
Cabin quality	240000Kg
Tower quality	347460Kg
Rotor diameter	126m
Hub diameter	3m
Tower height	90m

Considering the turbulence of winds and waves, The TurbSim was used to compile the new wind file as shown in Figure 4. Directing attention to individual pitch control, a PID torque controller was employed. The ultimate pitch angles were composed of two parts. A collective pitch control in the strategy was also testified with a PID controller on the feedback rotor speed in Figure 5.

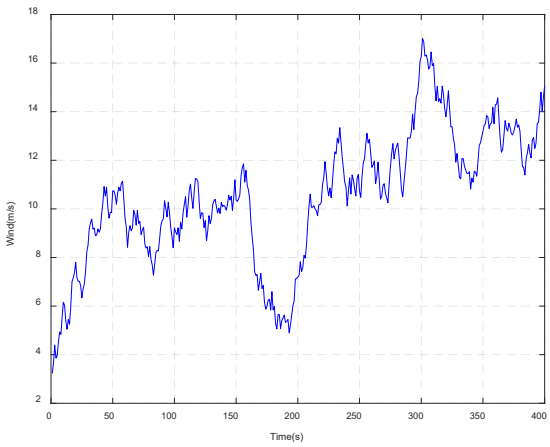

Figure 4. Turbulence wind used in simulation

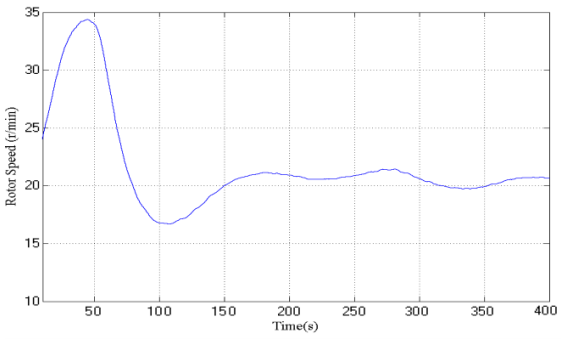

Figure 5. Rotor speed with PID in collective pitch control

The yaw moment and tilt moment are indicators of platform motion. The other part of the ultimate pitch angle is individual pitch control with the proposed algorithm to reduce the fatigue loads beyond the rated wind speed. Figure 6 and Fig 7 clearly and respectively contrasts the yaw moment

and the tilt moment of the suggested individual pitch control as well as the traditional collective pitch control. Tracking data for up to 400 seconds can demonstrate statistical significant. To further verify the memont reduction, the following deviation value μ are adopted:

$$\mu = \sum_{i=1}^{n} |y_i| / n \tag{34}$$

The deviation values of the tilt moment and the yaw moment are provided in Table 2.

Certainly, contributing to the loads' decrease, the optimized algorithm has effectively conducted the experiment, and especially when encountering strong turbulence, the moments were obviously reduced.

Table 2. The deviation values of the tilt moment and the yaw moment

The deviation values	Collective pitch control	Individual pitch control
The tilt moment	156.50	122.61
The yaw moment	114.94	75.57

5. Conclusion

Based on the promising FOWT, this study analyzed an advanced individual pitch control strategy. A data-driven predictive controller with feedforward compensation was implemented, concentrating on control design for the FOWT and wind turbine load models based control systems. Under identical and strict conditions, the introduced controller outperformed the traditional PID controller, ensuring the FOWT's stability and promoting its development. According to the simulation results, the feedforward-based algorithm might significantly facilitate floating platform stabilization

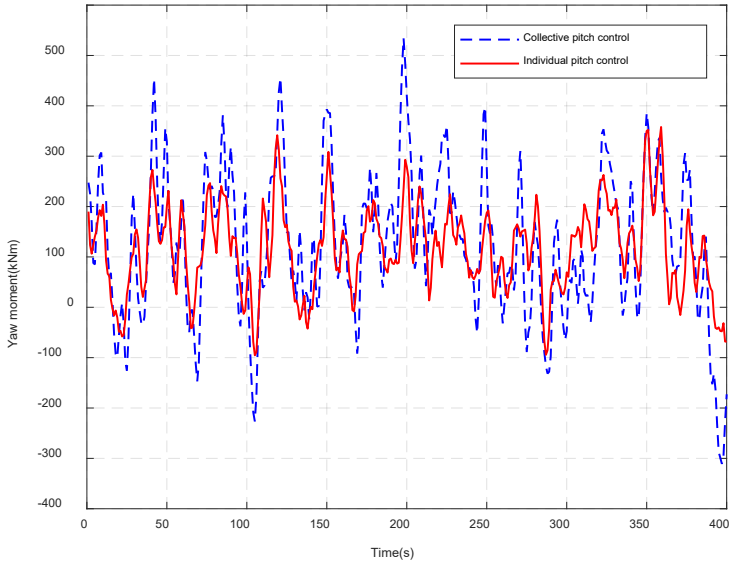

Figure 6. Result of yaw moment

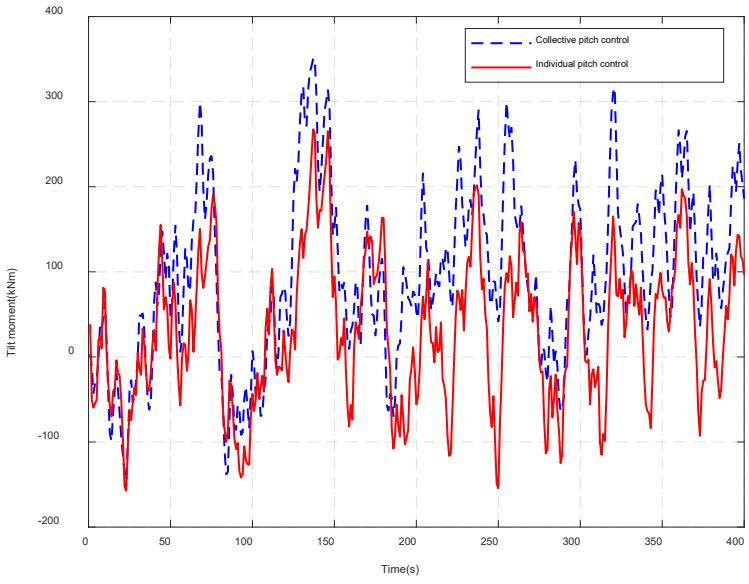

Figure 7. Result of tilt moment

Acknowledgements.

This research was funded by the Science and Technology Research Program of Chongqing Municipal Education Commission, grant number KJQN202301620 and Hybrid AI and Big Data Research Center of Chongqing University of Education (2023XJPT02).

References

[1] Z. Li, M. J. Liu, X. Cao, M. H. Gao, L. Y. Cheng, H. X. Sun. Aerodynamic performance analysis and power generation characteristics experiment of vertical axis wind turbine. Engineering Reports. 2022; vol. 4: e12500.

[2] O. A. Marzouk. Wind speed weibull model identification in Oman, and computed Normalized Annual Energy Production (NAEP) from wind turbines based on data from weather stations. Engineering Reports. 2025; vol. 7: e70089.

[3] M. Hu, J. Shi, S. Yang, M. Chen, Y. Tang, and S. Liu. Current status and future trends in installation, operation and maintenance of offshore floating wind turbines. Journal of Marine Science and Engineering. 2024; vol. 12, no. 12: 2155.

[4] X. Tong and X. W. Zhao. Vibration and power regulation control of a floating wind turbine with hydrostatic transmission. Renewable Energy. 2021; vol. 167: 899-906.

[5] B. Hand, A. Cashman. A review on the historical development of the lift-type vertical axis wind turbine: From onshore to offshore floating application. Sustainable Energy Technologies and Assessments. 2020; vol. 38: 100646.

[6] T. Jard, R. Snaiki. Real-time repositioning of floating wind turbines using model predictive control for position and power regulation. Wind. 2023; vol. 3, no. 2: 131-150.

[7] J. E. Sierra-Garcia, M. Santos. Improving wind turbine pitch control by effective wind neuro-estimators. IEEE Access. 2021; vol. 9: 10413-10425.

[8] A. A. Rostam-Alilou, C. W. Zhang, F. Salboukh, O. Gunes. Potential use of Bayesian Networks for estimating relationship among rotational dynamics of floating offshore wind turbine tower in extreme environmental conditions. Ocean Engineering. 2022; vol. 244: 110230.

[9] J. Yao, M. Xin. Finite-time suboptimal control design for aerobatic maneuver of variable-pitch quadrotor. IEEE Transactions on Aerospace and Electronic Systems. 2023; vol. 59, no. 4: 3736-3749.

[10] M. Mazare, M. Taghizadeh. Uncertainty estimator-based dual layer adaptive fault-tolerant control for wind turbines. Renewable Energy. 2022; vol. 188: 545-560.

[11] S. Christiansen, T. Knudsen, T. Bak. Optimal control of a ballast-stabilized floating wind turbine. 2011 IEEE International Symposium on Computer-Aided Control System Design (CACSD). IEEE, 2011.

[12] H. Namik, K. Stol. Performance analysis of individual blade pitch control of offshore wind turbines on two floating platforms. Mechatronics. 2011; vol. 21: 691-703.

[13] P. Venkaiah, B. K. Sarkar. Hydraulically actuated horizontal axis wind turbine pitch control by model free adaptive controller. Renewable Energy. 2020; vol. 147: 55-68.

[14] X. S. Luo. An individual pitch control method for floating offshore wind turbine. Journal of Physics: Conference Series. 2022; vol. 2276: 012032.

[15] S. T. Navalkar, E. van Solingen, J. W. van Wingerden. Wind tunnel testing of subspace predictive repetitive control for variable pitch wind turbines. IEEE Transactions on Control Systems Technology. 2015; vol. 23, no. 6: 2101-2116.

[16] Y. C. Liu, R. Ferrari, J. W. van Wingerden. Load reduction for wind turbines: an output-constrained, subspace predictive repetitive control approach. Wind Energy Science. 2022; vol. 7, no. 2: 523-537.

[17] Y. C. Liu, J. Frederik, R. M. G. Ferrari, P. Wu, S. W. Li, J. W. van Wingerden. Fault-tolerant individual pitch control of floating offshore wind turbines via subspace predictive repetitive control. Wind Energy. 2021; vol. 24, no. 9: 1045-1065.

[18] P. Wu, Y. C. Liu, R. M. G. Ferrari, J. W. van Wingerden. Floating offshore wind turbine fault diagnosis via regularized dynamic canonical correlation and fisher discriminant analysis. IET Renewable Power Generation. 2021; vol. 15, no. 16: 4006-4018.